

THE ORBITAL STRUCTURE OF DARK MATTER HALOS WITH GAS

ANDISHEH MAHDAVI

Harvard-Smithsonian Center for Astrophysics, MS 10, 60 Garden St., Cambridge, MA 02138;
 amahdavi@cfa.harvard.edu

Submitted April 11, 2000; Accepted August 2, 2000 for publication in the Astrophysical Journal

ABSTRACT

With the success of the *Chandra* and *XMM* missions and the maturation of gravitational lensing techniques, powerful constraints on the orbital structure of cluster dark matter halos are possible. I show that the X-ray emissivity and mass of a galaxy cluster uniquely specify the anisotropy and velocity dispersion profiles of its dark matter halo. I consider hydrostatic as well as cooling flow scenarios, and apply the formalism to the lensing cluster CL0024+16 and the cooling flow cluster Abell 2199. In both cases, the model predicts a parameter-free velocity dispersion profile that is consistent with independent optical redshift surveys of the clusters.

Subject headings: Galaxies: clusters: general—hydrodynamics—cooling flows—X-rays:
 galaxies—galaxies: clusters: individual (CL0024+16, Abell 2199)

1. INTRODUCTION

In the standard picture, a cluster of galaxies consists of a dark matter halo accompanied by galaxies and a hot, 1-15 keV plasma. The techniques for measuring the mass of the halo usually focus exclusively on the motions of the galaxies in the cluster, on the emissivity and temperature of the X-ray emitting gas, or on the gravitational lensing of distant sources by the halo. In this paper I show that combining these various data can place strong constraints on the velocity structure of the cluster dark matter halo.

Over the past two decades, a great deal of evidence has mounted that the X-ray emissivity ϵ of the plasma for many clusters is well fit by the particularly simple function (e.g. Jones & Forman 1984; Mohr, Mathiesen, & Evrard 1999)

$$\epsilon \propto \left(1 + \frac{r^2}{r_c^2}\right)^{-3\beta}. \quad (1)$$

This function is often referred to as the β -model in the literature; it has a core radius, r_c , and a faint end slope, β .

It is instructive to review the physical basis for the form of the β -model (see, e.g. Sarazin 1988). The starting point is the assumption that the plasma is in equilibrium with the dark matter potential. The general form of the equation of hydrostatic equilibrium is

$$\nabla P = -\rho_g \nabla \phi, \quad (2)$$

where P is the gas pressure, ρ_g is the gas density, and ϕ is the gravitational potential. With the assumption that the plasma is a spherically symmetric ideal gas, the equation becomes

$$\frac{1}{\rho_g} \frac{d}{dr} \left(\frac{\rho_g k_B T}{m_p \mu} \right) = -\frac{GM}{r^2} \quad (3)$$

where T is the plasma temperature, M is the total mass inside the radius r , m_p is the proton mass, μ is the mean molecular weight, and k_B is Boltzmann's constant. The dynamics of the dark matter halo, on the other hand,

are determined by the Jeans equation (e.g. Binney & Tremaine 1987, p. 204),

$$\frac{1}{\rho_{\text{dm}}} \frac{d}{dr} (\rho_{\text{dm}} \sigma_r^2) + \frac{2\eta \sigma_r^2}{r} = -\frac{GM}{r^2}. \quad (4)$$

Here $4\pi r^2 \rho_{\text{dm}} = dM/dr$ is the dark matter density, σ_r is the dark matter radial velocity dispersion, and η is the anisotropy parameter¹, which describes, in an average sense, the nature of the orbits of the dark matter particles. The anisotropy parameter is a dimensionless quantity equal to $1 - \sigma_\theta^2/\sigma_r^2$, where σ_θ^2 is the tangential velocity dispersion. When $\eta = 1$, the dark matter orbits are completely radial; when $\eta = -\infty$, the orbits are completely tangential; and when $\eta = 0$, the orbits are isotropic. Note that equation (4) is not the same as the galaxy Jeans equation, which involves the galaxy number density ν_{gal} in place of the dark matter density ρ_{dm} .

Three critical assumptions shape the derivation of the β -model. The first is that the gas is isothermal, and the second is that the dark matter orbits are perfectly isotropic. Then, equating (3) and (4),

$$\frac{d \ln \rho_g}{d \ln r} = \frac{d \ln \rho_{\text{dm}}}{d \ln r} \frac{\mu m_p \sigma_r^2}{k_B T}. \quad (5)$$

The final assumption is that the dark matter halo is nearly an isothermal sphere, with a density profile given by a King model, $\rho_{\text{dm}} \propto (1 + r^2/r_c^2)^{-3/2}$. Then the above equation has $\rho_g \propto (1 + r^2/r_c^2)^{-3\beta/2}$, with $\beta \equiv \mu m_p \sigma_r^2 / (k_B T)$. The isothermal emissivity, proportional to the square of the gas density, is then given by equation (1).

There is an inconsistency in the above derivation. The assumption that $\eta = 0$ everywhere is not compatible with a constant velocity dispersion σ_r , easily verified by inserting a King model into equation (4), setting $\eta = 0$, and noticing that σ_r must vary with the radius. Yet the β -model derived in this manner continues to provide an adequate empirical description of cluster emissivities.

¹In the stellar dynamics literature, which precedes the discussion of X-ray clusters by many decades, it is β that denotes the anisotropy parameter. But because the β is so widely used by X-ray astronomers to refer to the faint-end slope of the emissivity, I must switch symbols.

It is interesting to ask what anisotropy profiles $\eta(r)$ and velocity dispersion profiles $\sigma_r^2(r)$ are fully consistent with the β -model taken in conjunction with auxiliary measurements, e.g. gravitational lensing. A further impetus for investigating η is the recent development (e.g. Geller, Diaferio, & Kurtz 1999) that the density profiles of some clusters of galaxies are well fit by a cuspy model suggested by Navarro, Frenk, & White (1997; NFW); see Table 1. Because gasdynamical N-body simulations indicate that a β -model gas can coexist with an NFW dark halo (e.g. Eke et al. 1998), an analytic exploration of the basic equilibrium properties of the anisotropy parameter is appropriate. Finally, a theoretically sound functional form for η is required for analyzing cluster velocity dispersion profiles using the Jeans equations (e.g., Carlberg et al. 1997).

In this paper I develop a formalism for calculating $\eta(r)$ and $\sigma_r^2(r)$ simultaneously. I assume that the cluster is spherically symmetric, that the gas is in hydrostatic or quasihydrostatic equilibrium with the dark matter, that dark matter dominates the cluster potential, and that the gas temperature is always proportional to the local dark matter velocity dispersion. In §2 I derive the basic equations; in §3, I apply the model to hydrostatic plasmas and the cluster CL0024+16; in §4, I consider anisotropy profiles within quasihydrostatic cooling flows, specifically the cluster Abell 2199; and in §5 I summarize.

2. DERIVATION

The aim of this derivation is to solve the dark matter Jeans equation (4) for the radial velocity dispersion σ_r and the orbital anisotropy parameter η given a mass profile M . Because there are two unknown functions and only one equation, auxiliary assumptions are necessary. One approach is to make η a constant (Mahdavi et al. 1999; van der Marle 2000) and solve for $\sigma_r(r, \eta)$. However, N-body simulations suggest that the orbital distribution of the dark matter particles varies considerably throughout the halo (e.g. Kaufmann et al. 1999; Diaferio 2000). Another method involves assuming a functional form for the phase space distribution of the dark matter particles (Merritt 1985; Gerhard et al. 1998). This approach is tantamount to fixing the form of $\eta(r)$.

Here I outline a third approach that places no requirements on η itself. Instead I assume that the total specific energy of the dark matter particles is everywhere proportional to that of the plasma: $T \propto \sigma_{\text{tot}}^2$. This scaling law is not arbitrary, but is grounded in observations of groups and clusters of galaxies. Combined X-ray and optical observations of these systems have found that the mean emission-weighted gas temperature scales roughly as the second power of the total galaxy velocity dispersion (Mulchaey & Zabludoff 1998; Xue & Wu 2000). These data show that in many clusters, the dark matter, gas, and the galaxies are in dynamical equilibrium, with the specific energy of each component proportional to that of the other two at all observable radii.

Now I describe the implications of $T \propto \sigma_{\text{tot}}^2$ for the anisotropy parameter. In a spherically symmetric dark matter halo, the velocity dispersion tensor is close to diagonal in spherical coordinates. The local energy per unit mass is therefore given by the trace of the tensor, the total

three-dimensional velocity dispersion:

$$\sigma_{\text{tot}}^2 = \sigma_r^2 + \sigma_\theta^2 + \sigma_\phi^2 \quad (6)$$

$$= \sigma_r^2 (3 - 2\eta), \quad (7)$$

where σ_θ and σ_ϕ are the tangential and azimuthal velocity dispersions, respectively. In spherically symmetric systems, $\sigma_\theta = \sigma_\phi$ and $\eta = 1 - \sigma_\theta^2/\sigma_r^2$. Then the hypothesis that $T \propto \sigma_{\text{tot}}^2$ implies the following relationship between the gas temperature and the velocity dispersion:

$$3\beta_{\text{true}}k_B T = \mu m_p \sigma_r^2 (3 - 2\eta), \quad (8)$$

where β_{true} is a dimensionless constant.

Equations (3), (4), and (8) now form a closed set, solvable as follows. I begin by writing the equation of hydrostatic equilibrium in a different form:

$$\frac{d \ln \rho_g T}{d \ln r} = -\frac{GMm_p \mu}{k_B T r} \quad (9)$$

In clusters of galaxies, the plasma radiates chiefly through thermal bremsstrahlung, a collisional process whose total emissivity scales roughly as the square root of the temperature: $\epsilon \propto \rho_g^2 \sqrt{T}$. It follows that

$$\ln \rho_g = \frac{1}{2} \ln \epsilon - \frac{1}{4} \ln T + \text{constant}. \quad (10)$$

It is then possible to reformulate equation (9) in terms of the observed emissivity:

$$\frac{3}{4} \frac{d \ln T}{d \ln r} + \frac{1}{2} \frac{d \ln \epsilon}{d \ln r} = -\frac{GMm_p \mu}{k_B T r}. \quad (11)$$

This relation implies that, for isothermal plasmas, there is a one-to-one correspondence between the measured emissivity profile and the mass profile. In other words, an isothermal sphere of ideal gas with a measured emissivity profile $\epsilon(r)$ must have the mass profile given by setting $d \ln T / d \ln r = 0$ in equation (11):

$$M(r) = -\frac{k_B T r}{2Gm_p \mu} \frac{d \ln \epsilon}{d \ln r}. \quad (12)$$

In general, the plasma can have a temperature gradient; the profile is given by the solution of equation (11):

$$T(r) = \frac{4\mu m_p}{3k_B \epsilon^{2/3}} \int_r^\infty \frac{GM}{r^2} \epsilon^{2/3} dr. \quad (13)$$

Here the constant of integration is chosen such that T converges as $r \rightarrow \infty$. The temperature at infinity is

$$T_\infty = -\lim_{r \rightarrow \infty} \frac{2GMm_p \mu}{k_B r} \left(\frac{d \ln \epsilon}{d \ln r} \right)^{-1}. \quad (14)$$

If the logarithmic derivative of the emissivity tends to a constant value, then as $r \rightarrow \infty$, (1) $T_\infty = 0$ unless $M(r) \propto r$, and (2) $M(r) \propto r$ is the steepest mass profile allowed. A further useful result is obtained by applying l'Hôpital's rule to the derivative of equation 13:

$$\lim_{r \rightarrow \infty} \frac{d \ln T}{d \ln r} = \lim_{r \rightarrow \infty} \frac{d \ln M}{d \ln r} - 1. \quad (15)$$

That is, $T(r) \propto M(r)/r$ asymptotically. Because the mass can never decrease, the temperature never falls faster than r^{-1} at large radii.

Now I rewrite the Jeans equation for a spherically symmetric system of collisionless particles:

$$\frac{d \ln \rho_{\text{dm}} \sigma_r^2}{d \ln r} + 2\eta = -\frac{GM}{\sigma_r^2 r}, \quad (16)$$

Using equation (8), it is possible to eliminate η :

$$\frac{d \ln \rho_{\text{dm}} \sigma_r^2}{d \ln r} + 3 \left(1 - \frac{\beta_{\text{true}} k_B T}{m_p \mu \sigma_r^2} \right) = -\frac{GM}{\sigma_r^2 r}. \quad (17)$$

This equation has the solution

$$\sigma_r^2(r) = 3\beta_{\text{true}} \sigma_1^2 - \sigma_2^2, \quad (18)$$

$$\sigma_1^2 = \frac{1}{r^3 \rho_{\text{dm}}} \int \frac{k_B T}{m_p \mu} r^2 \rho_{\text{dm}} dr, \quad (19)$$

$$\sigma_2^2 = \frac{1}{r^3 \rho_{\text{dm}}} \int G M r \rho_{\text{dm}} dr. \quad (20)$$

The constant of integration should be zero in most cases, because a nonzero constant will usually introduce a $(r^3 \rho_{\text{dm}})^{-1}$ divergence in the velocity dispersion as $r \rightarrow 0$. Such a divergence cannot be reconciled with equation (8) if the temperature is finite at $r = 0$ and $\eta < 1$.

Two physical considerations limit the possible values of β_{true} . The first is that $\sigma_r^2 \geq 0$. Then

$$\sigma_2^2 \leq 3\beta_{\text{true}} \sigma_1^2. \quad (21)$$

The second consideration is $\eta < 1$, equivalent to requiring that the tangential velocity dispersion σ_θ^2 always be positive. Equation (8) then implies

$$3\beta_{\text{true}} k_B T \geq m_p \mu \sigma_r^2 \quad (22)$$

$$3k_B T \beta_{\text{true}} \geq m_p \mu (3\beta_{\text{true}} \sigma_1^2 - \sigma_2^2) \quad (23)$$

$$\sigma_2^2 \geq 3\beta_{\text{true}} \left(\sigma_1^2 - \frac{k_B T}{m_p \mu} \right) \quad (24)$$

Any physically acceptable emissivity-potential pair must simultaneously meet the requirements of inequalities (21) and (24) at all radii. Only values of β_{true} which meet these two constraints are valid. If at any two radii the two inequalities are in conflict, the emissivity-potential pair is not physically consistent with the assumptions of this derivation. Whenever $T \rightarrow 0$ asymptotically and $\sigma_{1,2}^2$ do not, the above inequalities force a unique value of β_{true} :

$$\beta_{\text{true}} = \lim_{r \rightarrow \infty} \frac{\sigma_2^2}{3\sigma_1^2}. \quad (25)$$

Finally, for a valid choice of β_{true} , the anisotropy profile is given by the inversion of equation (8):

$$\eta(r) = \frac{3}{2} \left(1 - \frac{\beta_{\text{true}} k_B T}{m_p \mu \sigma_r^2} \right). \quad (26)$$

Thus only the shapes, and not the normalizations, of the gravitational potential and the emissivity profile determine the velocity anisotropy.

3. HYDROSTATIC SOLUTIONS

Here I discuss the anisotropy solutions for clusters in perfect hydrostatic equilibrium—i.e., assuming radiative cooling is unimportant. I begin with potential-emissivity pairs described by simple power laws. Although single power laws do not provide a satisfactory description of real clusters, they elucidate the general properties of the solutions more clearly than broken power laws, for which the integrals in equations (19)-(20) are often not expressible in terms of elementary functions.

3.1. Power Law Mass and Emissivity Profiles

Consider a cluster with mass profile $M = Ar^\alpha$ (with $\rho_{\text{dm}} \propto r^{\alpha-3}$), and a power law emissivity profile $\epsilon \propto r^\nu$. The mass must never decrease with the radius, so $\alpha > 0$. Then equation (13) has the form

$$\frac{kT(r)}{m_p \mu} = \frac{4GA r^{\alpha-1}}{3(1-\alpha-2\nu/3)}. \quad (27)$$

It is unphysical for the temperature to become infinite at large radius. Furthermore, the temperature must always be positive. Hence we have the constraints

$$0 < \alpha \leq 1 \quad (28)$$

$$\nu < \frac{3-3\alpha}{2} \quad (29)$$

Thus, if the matter distribution behaves like a singular isothermal sphere ($\alpha = 1$), the plasma is isothermal as long as its emissivity is a declining power law of arbitrary index.

The radial velocity dispersion from equation (18) is

$$\sigma_r^2(r) = \frac{GA r^{\alpha-1}}{2\alpha-1} \left(\frac{4\beta_{\text{true}}}{\gamma} - 1 \right), \quad (30)$$

$$\gamma \equiv 1 - \alpha - 2\nu/3. \quad (31)$$

Again, for a singular isothermal sphere the radial velocity dispersion is constant regardless of the power law index of the emissivity. The logarithmic $\alpha = 1/2$ solution is not permitted, because it gives $\eta = 3/2$ at $r = 0$.

Substituting equations (27) and (31) into the anisotropy equation (26) yields,

$$\eta = \frac{1}{2} \left(3 - \frac{8\alpha-4}{4-\gamma/\beta_{\text{true}}} \right). \quad (32)$$

Thus the anisotropy parameter η is always constant for the permitted power law mass and emissivity profiles. Note that the dark matter orbits are perfectly isotropic ($\eta = 0$) only if the ratio of the dark matter velocity dispersion to the gas temperature is

$$\beta_{\text{true}} = \frac{3\gamma}{16-8\alpha}. \quad (33)$$

Not all values of β_{true} are allowed. The requirements that $\sigma_r^2 > 0$ and $\eta < 1$ place the following bounds on β_{true} :

$$\frac{\gamma}{8-8\alpha} < \beta_{\text{true}} < \frac{\gamma}{4} \quad \text{if } \alpha < 1/2; \quad (34)$$

$$\frac{\gamma}{4} < \beta_{\text{true}} < \frac{\gamma}{8-8\alpha} \quad \text{if } \alpha > 1/2. \quad (35)$$

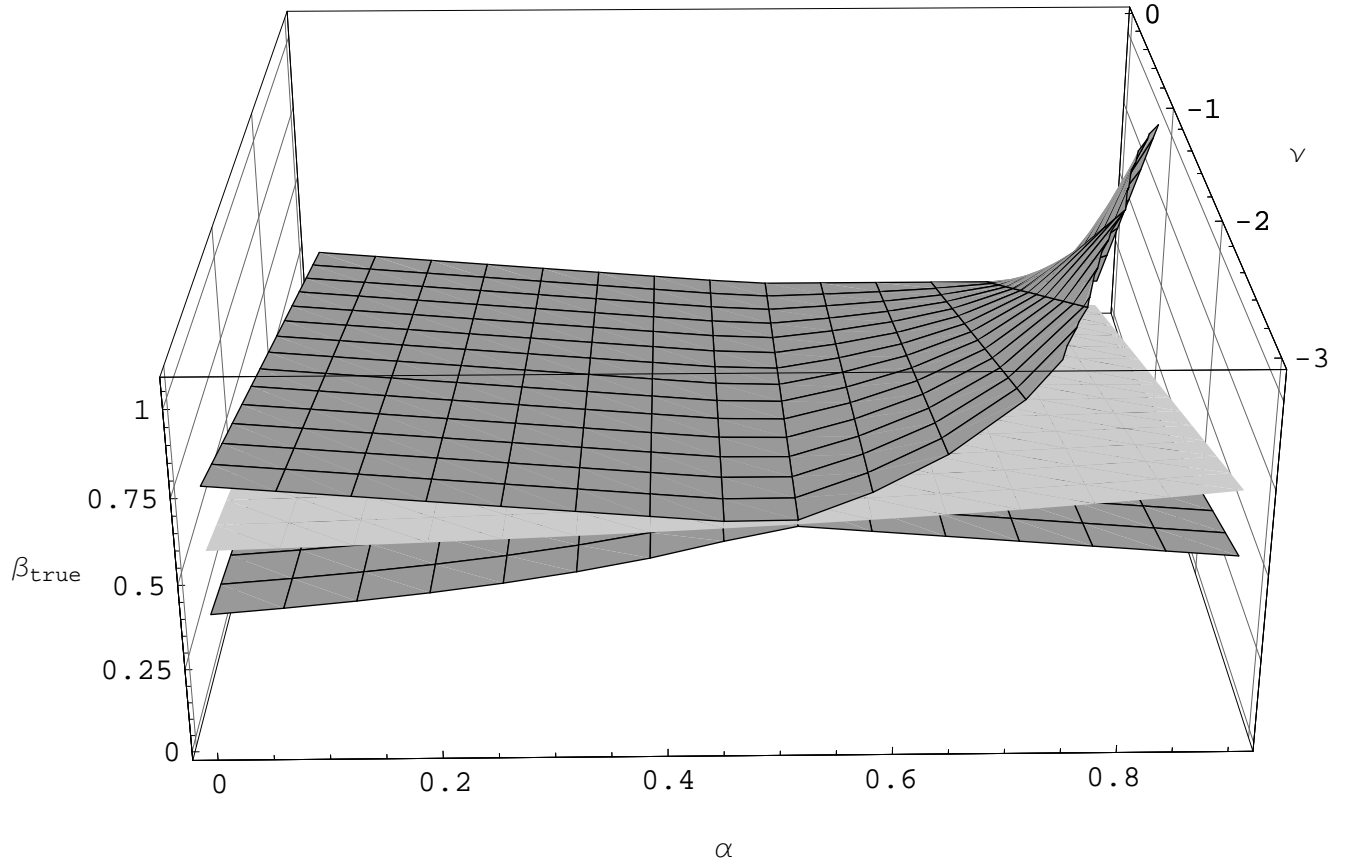
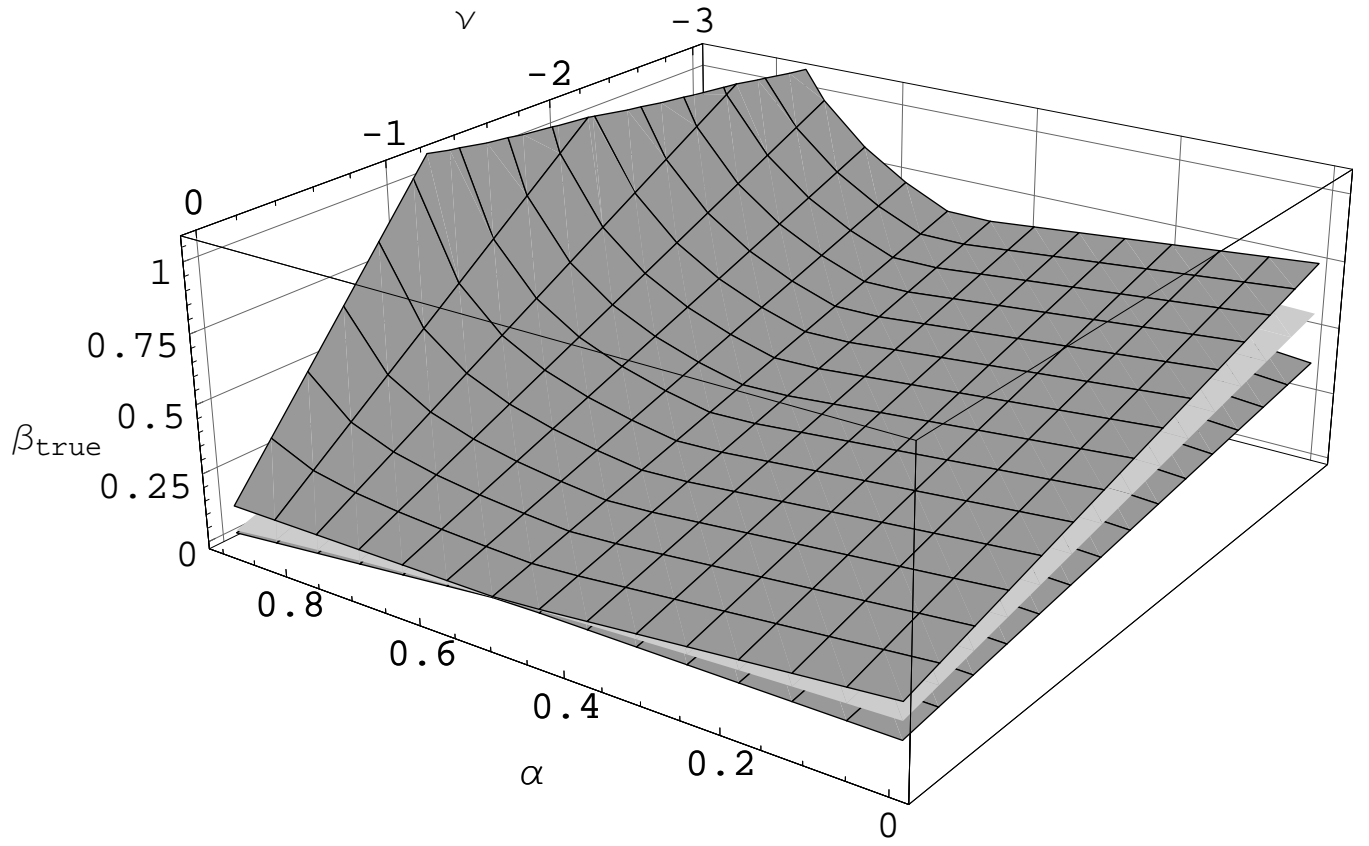


FIG. 1.— Limits on β_{true} , the ratio of the total dark matter velocity dispersion to the gas temperature, for mass and emissivity profiles $M \propto r^\alpha$ and $\epsilon \propto r^\nu$. Two different views of the same plot are shown for clarity. The meshed surfaces indicate the upper and lower limits on β_{true} . The smooth surface shows the required value of β_{true} such that the velocity anisotropy $\eta = 0$.

Figure 1 depicts these boundaries, as well as the $\eta = 0$ criterion. For $\alpha < 1$, β_{true} always has firm upper and lower limits, but for the singular isothermal sphere, arbitrary large values of β_{true} are allowed. Within the upper and lower limits, the anisotropy η takes on the full range of allowed values, $(-\infty, 1)$.

A physical explanation of overall tilt of the planes in Figure 1 lies in the slope of the emissivity profile. When the gas distribution is relatively extended ($\nu \gtrsim -1$), the gas is on the average hotter, and the dark matter to gas energy ratio β_{true} is smaller, than when the gas is relatively concentrated ($\nu < -1$). Thus the mean permitted value for β_{true} increases as the emissivity profile steepens.

The asymmetry in Figure 1 between the boundaries for $\alpha < 1/2$ and $\alpha > 1/2$ is related to the differences in the circular velocity profile of the potential, $v_c = \sqrt{GM/r}$. In systems with $\alpha > 1/2$, v_c is nearly constant, and ample kinetic energy is available at all radii to particles with tangential orbits. It is therefore statistically difficult to underpopulate the tangential orbits and achieve $\eta \approx 1$. Thus β_{true} must be inordinately large to achieve a significant radial anisotropy: a large amount of kinetic energy must reside in the radial orbits for them to dominate the total velocity dispersion.

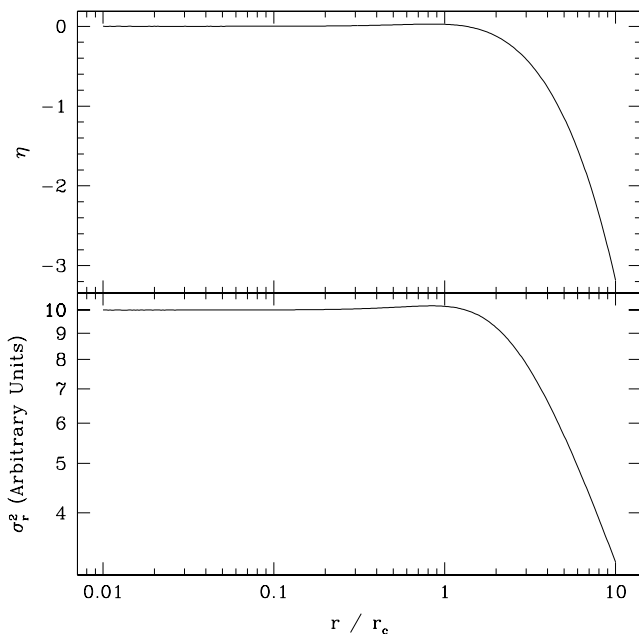


FIG. 2.— Anisotropy profile (top) and radial velocity dispersion profile (bottom) for the isothermal β -model.

3.2. Isothermal β -models

The mass and emissivity profiles of real clusters are better described by broken power laws. The β -model emissivity, which has $\epsilon \propto (1 + x^2)^{-3\beta}$, where $x \equiv r/r_c$, fits many clusters without cooling flows, and is commonly taken to describe an isothermal gas. If the temperature is constant, and the plasma is in hydrostatic equilibrium with the gravitational potential, then according to equation (12) the mass profile has to be

$$M(r) = \frac{3\beta k T r_c}{m_p \mu G} \frac{x^3}{1 + x^2}, \quad (36)$$

different from the mass profile of the King sphere (Table 1). The reason for this discrepancy is that the classical derivation of the β -model emissivity assumes that the King sphere is isothermal (see the Introduction). But the King sphere is only an approximation to the true nonsingular isothermal sphere (Binney & Tremaine 1987, p. 228). For a β -model gas to be truly isothermal, it must be embedded in the mass profile given by equation (36).

It is then straightforward to derive the orbital properties of the spherically symmetric dark matter halo using the equations derived in §2. They yield $\beta_{\text{true}} = \beta$, and

$$\sigma_r^2(r) = \frac{3\beta k T}{4m_p \mu x^2} \left[\frac{3(1 + x^2)^2 \tan^{-1} x}{x(3 + x^2)} - 1 \right]. \quad (37)$$

The central velocity dispersion is $\sigma_r^2(0) = \beta k T / (m_p \mu)$, and as $r \rightarrow \infty$, $\sigma_r^2 \sim 1/r$. Because the radial velocity dispersion eventually vanishes, the orbits at $r = \infty$ must be completely tangential to keep the total velocity dispersion constant, and therefore $\eta \rightarrow -\infty$. The required anisotropy parameter is independent of β :

$$\eta(r) = \frac{3}{2} - \frac{2x^3(3 + x^2)}{3(1 + x^2)^2 \tan^{-1} x - x(3 + x^2)}. \quad (38)$$

Figure 2 shows the velocity dispersion and anisotropy profiles for the isothermal β -model.

3.3. Non-isothermal β -models

Although many clusters of galaxies contain an isothermal plasma, a perhaps larger fraction exhibit temperature gradients. For example, all but 3 of the 24 clusters examined with *ASCA* by Markevitch et al. (1998) have projected temperature profiles which decline with radius.

A temperature gradient results whenever a β -model emissivity is in equilibrium with a mass distribution different from equation (36). Here I calculate the anisotropy solutions for the β -model together with the various profiles listed in Table 1.

Figure 3 shows the equilibrium temperature profiles given by equation (13) for $\beta = 0.65$ and $\beta = 1$. Here the temperature always rises towards the core, but only because r_c is the same for both the emissivity and the matter density. Were r_c to be different for the two profiles (as in §3.4 below), the temperature could still fall towards the center. Note that the King approximation to the isothermal sphere, from which the β -model is derived, has constant temperature only within several core radii; at larger radii the plasma temperature drops steeply. Conversely, the dark matter potential of a singular isothermal sphere causes the β -model gas to have a temperature gradient inside the core, but a constant temperature at large radii. As one would expect, the gas in a cluster with $\beta = 0.65$ is on the average hotter than the gas in a cluster of the same mass but with $\beta = 1$.

The next step is to decide which values of β_{true} , the ratio of the total dark matter energy to the gas energy, are appropriate. Figure 4 shows the upper and lower limits for the singular isothermal sphere from equations (21) and (24). Because no single value of β_{true} can simultaneously satisfy the limits at all radii, the SIS and the β -model are an incompatible potential-emissivity pair.

TABLE 1
MASS PROFILES CONSIDERED

Profile	$\rho(x)$	$M(x)$
SIS	x^{-2}	$\frac{x}{\sqrt{1+x^2}}$
King	$(1+x^2)^{-3/2}$	$\ln(x + \sqrt{1+x^2}) - x/\sqrt{1+x^2}$
NFW	$x^{-1}(1+x)^{-2}$	$\ln(1+x) - x/(1+x)$
Hernquist	$x^{-1}(1+x)^{-3}$	$x^2(1+x)^{-2}$
Plummer	$(1+x^2)^{-5/2}$	$x^3(1+x^2)^{-3/2}$

NOTE.—The density and mass profiles are given without normalization and in terms of the scaled radius $x \equiv r/r_c$.

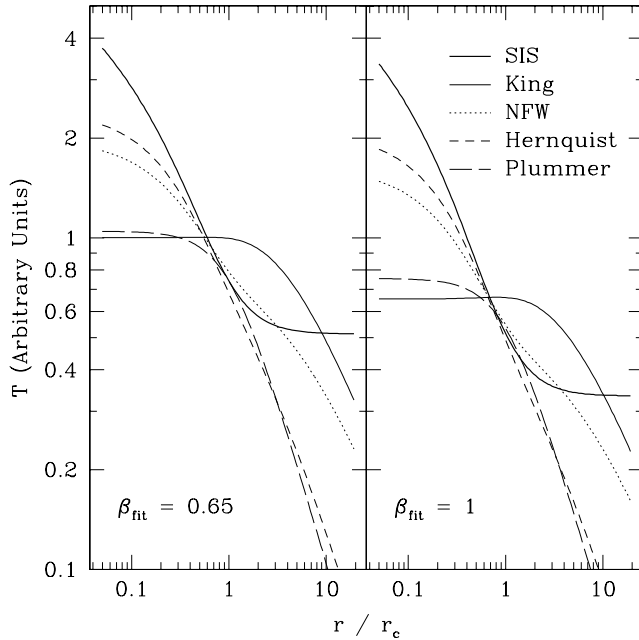


FIG. 3.— The equilibrium temperature profile for two β -model emissivity profiles and various gravitational potentials. The mass profiles are normalized so that they all contain the same amount of mass within $r = r_c$.

However, as Figure 5 shows, the rest of the mass profiles in Table (1) have admissible solutions when combined with a β -model gas. In contrast to the scale-free solutions in §3.1, equations (21) and (24) allow one unique value of β_{true} for each potential:

$$\beta_{\text{true}} = \lim_{r \rightarrow \infty} \frac{\sigma_2^2}{3\sigma_1^2}. \quad (39)$$

In general, the function $\beta_{\text{true}}(\beta)$, which matches the observed emissivity, characterized by β , with the physical energy ratio β_{true} , is not analytic. However, the integrals in equation (19) and (20) do have analytic representations for a β -model gas embedded in a Plummer sphere. The exact relations are

$$T(x) \propto \frac{4}{3(4\beta + 1)\sqrt{1+x^2}}, \quad (40)$$

$$\beta_{\text{true}} = \frac{4\beta + 1}{8}, \quad (41)$$

$$\sigma_r^2(x) \propto \frac{1}{6\sqrt{1+x^2}} \quad (42)$$

$$\eta(r) = 0, \quad (43)$$

where $x \equiv r/r_c$.

The Plummer model is remarkably well matched to the β -model gas emissivity. Its velocity dispersion is always independent of β , and the dark matter orbits are completely isotropic. This result is surprising and counterintuitive, because the β -model emissivity is historically derived from the isotropic King model. But as I have discussed above, that derivation assumes that the perfectly isotropic King sphere is isothermal, an assumption which breaks down well outside the core. In contrast, though it is not isothermal, a β -model gas embedded in an $\eta = 0$ Plummer sphere satisfies the equations of hydrostatic equilibrium perfectly.

For the King, NFW, and Hernquist models $\beta_{\text{true}}(\beta)$ is also roughly linear, with the general property that $\beta_{\text{true}} < \beta$ in each case. The resulting radial velocity dispersion profiles, given by equation (18), and anisotropy profiles, given by equation (32), appear in Figures 6 and 7, respectively. For the King profiles, β correlates strongly with the orbital anisotropy at infinity; $\beta = 1$ gives almost completely radial orbits at infinity, $\beta = 0.65$ results in orbits with a greater tangential component, and $\beta = 3/4$ gives perfect isotropy at all radii.

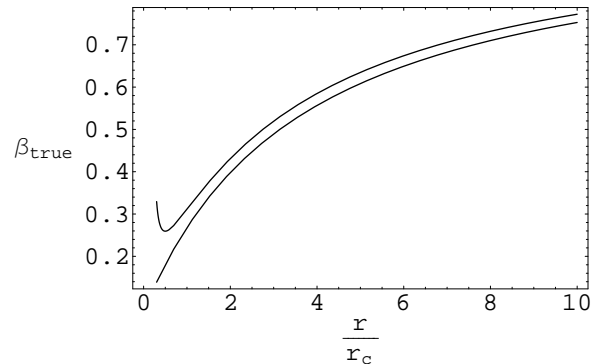


FIG. 4.— Upper and lower limits for β_{true} , the ratio of the dark matter energy to the gas energy, for a β -model gas embedded in a singular isothermal sphere. The figure shows that a constant β_{true} is not allowed.

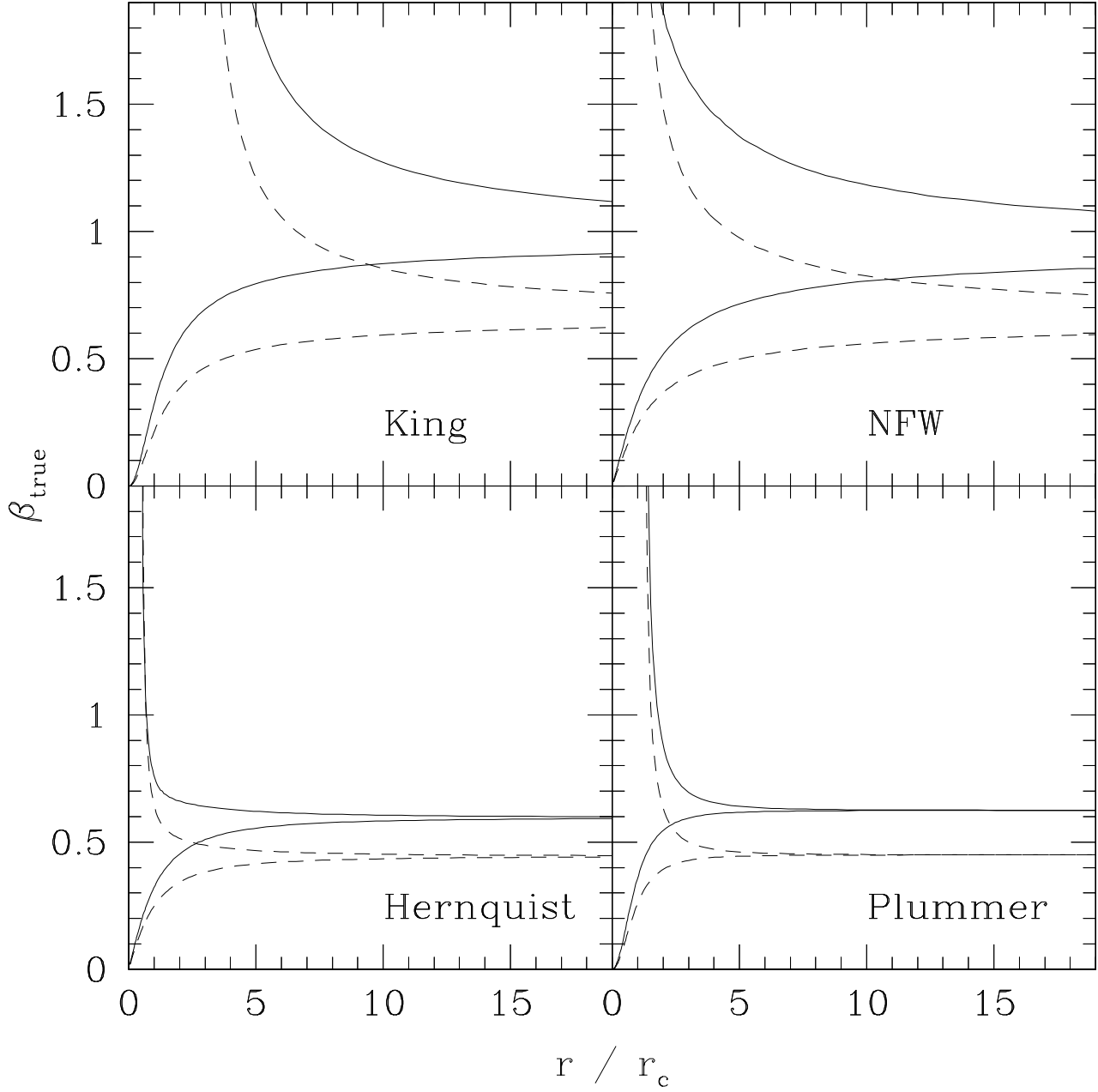


FIG. 5.— Upper and lower limits for β_{true} , the ratio of the dark matter energy to the gas energy, for a β -model emissivity combined with the various mass profiles listed in Table 1. Solid lines show $\beta = 1$, and dashed lines show $\beta = 0.65$.

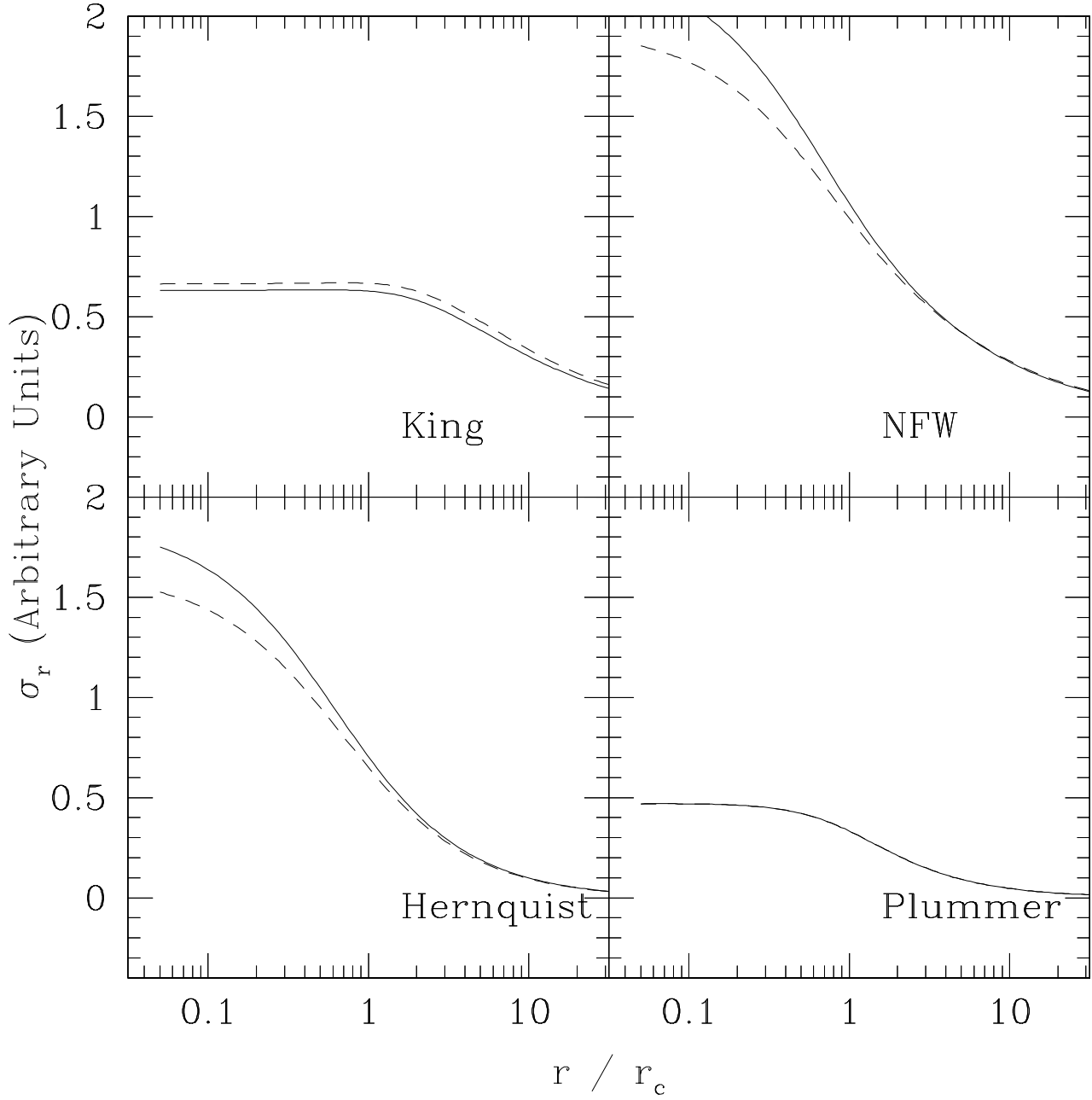


FIG. 6.— Radial velocity dispersion profiles for the various potentials in Table 1 when they contain a β -model gas. Solid lines show $\beta = 1$, and dashed lines show $\beta = 0.65$.

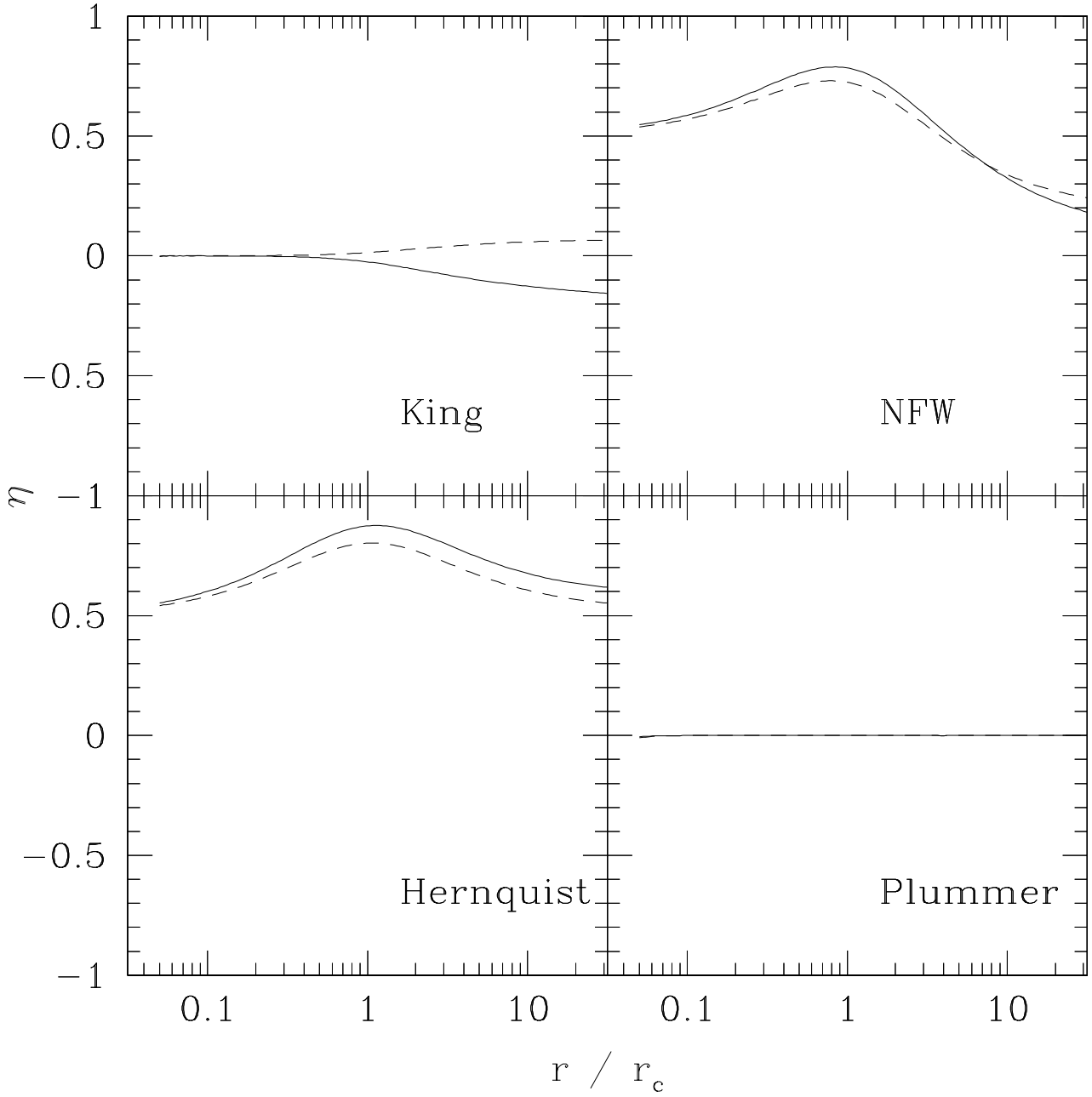


FIG. 7.— Anisotropy profiles for the various potentials in Table 1 when they contain a β -model gas. Solid lines show $\beta = 1$, and dashed lines show $\beta = 0.65$.

The anisotropy profiles of the NFW and Hernquist models show a particularly interesting structure. Both profiles have a small radial anisotropy at $r = 0$, attain a peak of $\eta \approx 0.75$ near $r = r_c$, and then decline towards a final, positive value.

The King and Plummer spheres exhibit featureless $\eta(r)$, whereas the NFW and Hernquist anisotropies have a maximum value. The physics behind this difference lies in the behavior of the dark matter density as $r \rightarrow 0$. The NFW and Hernquist profiles have a cuspy $\rho_{\text{dm}} \propto r^{-1}$ for $r \ll r_c$, whereas the King and Plummer spheres have finite density at $r = 0$. If the gas is in perfect hydrostatic equilibrium with the cuspy models, its temperature profile rises as $r \rightarrow 0$. For the dark matter to gas energy ratio β_{true} to be constant, the total velocity dispersion $\sigma_{\text{tot}}^2 = \sigma_r^2(3 - 2\eta)$ must then rise towards the center as well. But σ_r^2 is also coupled to the temperature and mass distribution via the Jeans equation (16). For $r < r_c$, the temperature term σ_1^2 from equation (19) dominates. Because of the density cusp at $r < r_c$, σ_1^2 itself falls more slowly than the temperature, and an increasing radial anisotropy is required to compensate, keeping β_{true} constant. At larger radii $r > r_c$, however, the subtractive, gravitational term σ_2^2 competes with the temperature term and causes σ_r^2 to fall rapidly. A larger tangential velocity component is then required to maintain a constant dark matter to gas energy ratio, and $\eta(r)$ falls.

Remarkably, the NFW and Hernquist anisotropies in Figure 7 are similar to the dark matter anisotropy profiles in N-body simulations without gas (Cole & Lacey 1996; Kauffman et al. 1999; Diaferio 1999). In these simulations, $\eta(r)$ is positive at $r = 0$, achieves a maximum near the virial radius, and then decreases to negative values. The close correspondence between the results of this derivation, which rely closely on the structure of the X-ray emitting gas in the dark matter halos, and the N-body simulations, which do not include gas physics, is encouraging.

3.4. Application to CL0024+16

Now I use X-ray imaging, gravitational lensing, and an optical redshift survey to test the simple hydrostatic formalism developed above. I derive unique velocity dispersion and anisotropy profiles by combining X-ray and lensing data for CL0024+16. I calculate the shape and normalization of the dark matter velocity dispersion profile without recourse to any free parameters. This profile, once projected, can be directly compared to the independent galaxy velocity dispersion profile, providing a powerful consistency test of the complete dynamical model.

CL0024+16, a $z = 0.39$ cluster, has *ROSAT* High Resolution Imager X-ray data (Böhringer et al. 2000), an *ASCA* temperature measurement (Soucail et al. 2000), and a mass profile from strong lensing (Tyson, Kochanski, & Dell’Antonio 1998). These observations independently fix the X-ray emissivity and the mass profile. Furthermore, a catalog of optical redshifts for 138 galaxies in the field of the cluster is available (Dressler et al. 1999).

The Tyson et al. (1998) surface mass density is characterized by a soft core within the lensing radius r_l :

$$\Sigma(R) = K_1 \frac{(1 + \gamma R^2/r_l^2)}{(1 + R^2/r_l^2)^{2-\gamma}}, \quad (44)$$

where R is the projected distance from the cluster center,

$K_1 = 7900 h_{100} M_\odot \text{ pc}^{-2}$ is the central surface density, the slope $\gamma = 0.57$, and $r_l = 35 h_{100}^{-1} \text{ kpc}$, with the Hubble Constant $H_0 = 100 h_{100} \text{ km s}^{-1} \text{ Mpc}^{-1}$. Outside the lensing radius r_l the mass profile resembles an NFW profile with a core radius $r_c = 311 h_{100}^{-1} \text{ kpc}$:

$$\Sigma(R) = \frac{M}{2\pi r_c^2 (R^2/r_c^2 - 1)} \left(1 - \frac{\sec^{-1} R/r_c}{\sqrt{R^2/r_c^2 - 1}} \right). \quad (45)$$

Here M is determined by requiring continuity with equation (44). Thus the density profile of CL0024+16 resembles that of a NFW halo, but lacks a central singularity.

The deprojected density profile is given by (Binney & Tremaine 1987, p. 205):

$$\rho_{\text{dm}}(r) = -\frac{1}{\pi} \int_r^\infty \frac{d\Sigma}{dR} \frac{dR}{\sqrt{R^2 - r^2}}. \quad (46)$$

This integral is well approximated by the function,

$$\rho_{\text{dm}}(r) = \frac{107.5 h_{100}^2}{(1 + r/r_0)^3} \times 10^{15} M_\odot \text{ Mpc}^{-3}, \quad (47)$$

where $r_0 = 0.0725 h_{100}^{-1} \text{ Mpc}$. The resultant projected mass profile is better than 12% accurate everywhere within the lensing arcs, commensurate with the $\approx 15\%$ error in the Tyson et al. (1998) parameters. The X-ray emissivity, on the other hand, is well described by a β -model with core radius $33 h_{100}^{-1} \text{ kpc}$ and $\beta = 0.475$ (Böhringer et al. 2000).

Because the central cooling time of the CL0024+16 is approximately the same as the age of the cluster, it should not contain a cooling flow (Soucail et al. 2000). Therefore the hydrostatic analysis discussed in the previous sections is appropriate. I take the mean molecular weight to be $\mu = 0.6$. Note that of all the properties derived by the model, only the temperature depends on the choice of μ . Figure 8 shows the results.

According to the model, the central temperature of the cluster should be $\approx 9.2 \text{ keV}$. The emission-weighted temperature within the *ASCA* aperture should be 12 keV; the Soucail et al. (2000) spectroscopic analysis gives a 90% confidence interval of 3.6–10.6 keV. Thus the predicted plasma temperature is consistent with but somewhat above the measurement. The discrepancy is not tied to the present analysis, but is an intrinsic property of the lensing and the X-ray data, which give only marginally consistent mass measurements for the cluster (Soucail et al. 2000). The lensing mass measurement might be an overestimate because of contamination by large scale structure projected along the line of sight (Metzler et al. 1999). The X-ray measurement is also suspect, because $\beta < 0.5$ in theory yields an infinite X-ray luminosity for the cluster.

Given the X-ray and lensing data, however, the calculations show that the dark matter to gas energy ratio is $\beta_{\text{true}} = 0.561$. Then it is straightforward to derive the anisotropy profile $\eta(r)$ and the radial velocity dispersion profile $\sigma_r^2(r)$ through equations (19)–(20). The line-of-sight dark matter velocity dispersion profile is (Binney & Tremaine 1987, p. 208)

$$\sigma_p^2(r) = \frac{2}{\Sigma} \int_R^\infty \left(1 - \eta \frac{R^2}{r^2} \right) \frac{\nu \sigma_r^2 r dr}{\sqrt{r^2 - R^2}}. \quad (48)$$

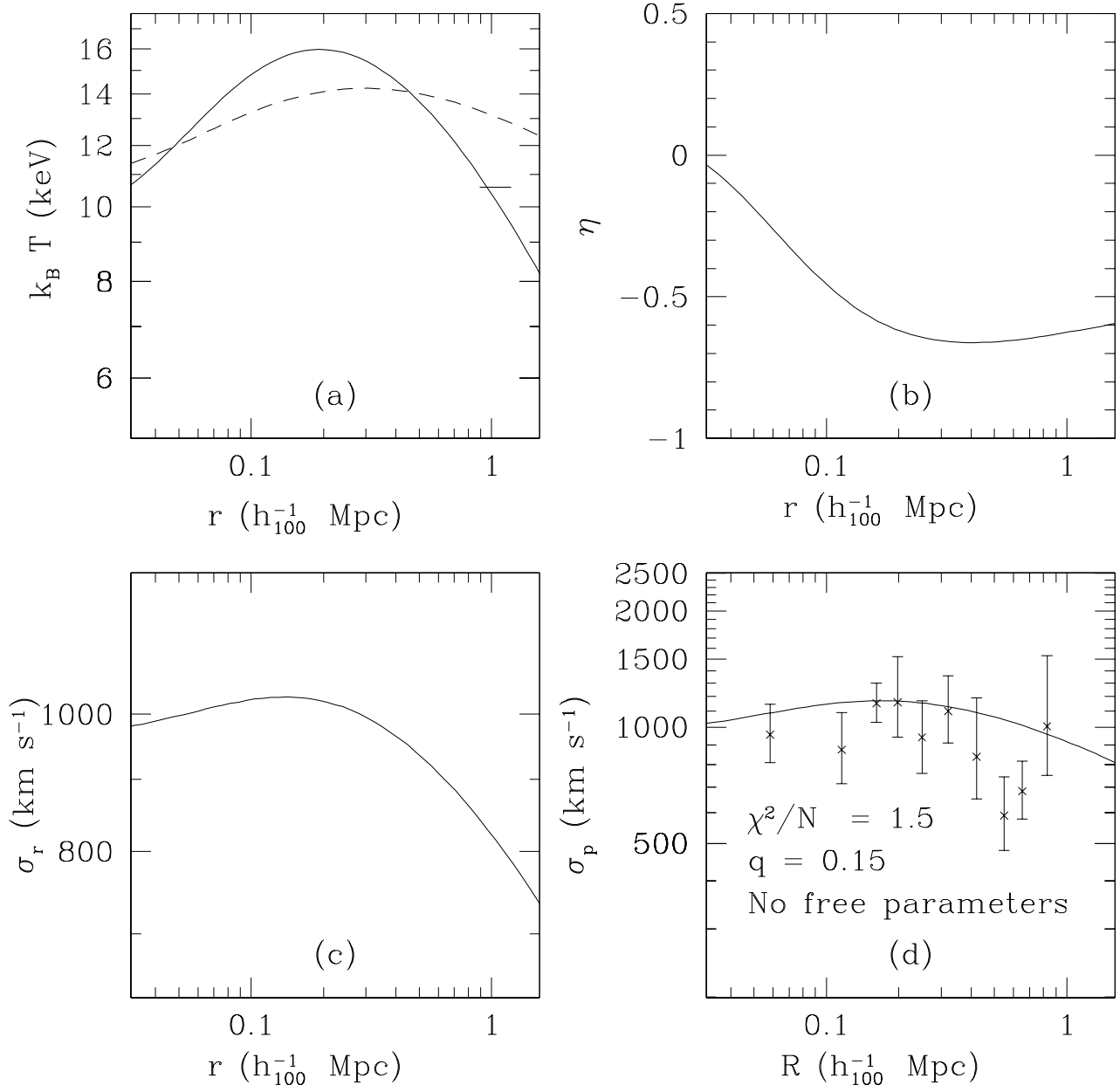


FIG. 8.— Derived properties of CL0024+16, and a comparison with the optical spectroscopic data: (a) predicted plasma temperature (solid line) and mean integrated emission-weighted temperature as observable by *ASCA* (dashed line); (b) predicted orbital anisotropy profile; (c) predicted three-dimensional radial velocity dispersion; (d) predicted line-of-sight velocity dispersion profile along with the measured galaxy velocity dispersion (Dressler et al. 1999).

The theoretical $\sigma_p(r)$ appears in Figure 8 alongside the line-of-sight velocity dispersion profile of the galaxies. To calculate $\sigma_p(r)$ from the Dressler et al. (1999) data, it is first necessary to determine the well-mixed cluster membership. I first select all Dressler et al. (1999) galaxies in the CL0024+16 field with redshifts $0.381 < z < 0.404$, corresponding to a $\pm 2500 \text{ km s}^{-1}$ line-of-sight velocity relative to the cluster rest frame. Then I apply the DEDICA algorithm (Pisani 1993) to determine the cluster membership. DEDICA uses Gaussian kernels to arrive at a maximum-likelihood estimate of cluster membership, in this case 104 galaxies. Finally, I measure $\sigma_p(r)$ by gathering the members into 10 bins of 10-11 galaxies, and calculating σ_p and its associated errors using standard bootstrap analysis.

The simple model discussed above well describes the velocity dispersion profile of CL0024+16. The χ^2 statistic is 15 for 10 degrees of freedom, yielding an acceptable fit quality $q = 0.15$ (Press et al. 1993, p. 660). The agreement is remarkable given that no free parameters are allowed in the comparison.

4. MULTIPHASE COOLING FLOW SOLUTIONS

4.1. General Properties

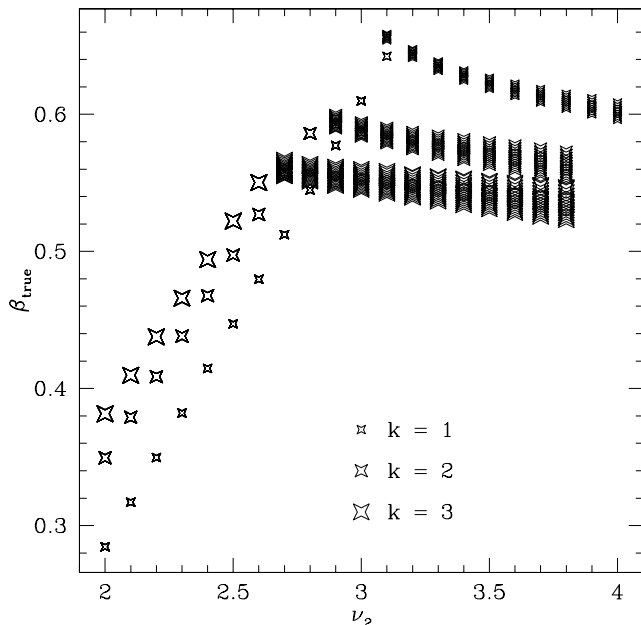


FIG. 9.— The dark matter to gas energy ratio, β_{true} , for cooling flow models with $k = 1, 2, 3$ and faint-end emissivity slopes ν_2 .

So far this discussion has focused on a intracluster plasma in hydrostatic equilibrium with the gravitational potential. This scenario provides a good description of most clusters, at least for gas removed more than ≈ 100 -200 kpc from the cluster center. However, the plasma in many clusters has a cooling time significantly shorter than the Hubble time within $r \approx 100$ kpc, an indication that an inward flow may be present. It is worth exploring how the dark matter anisotropy changes within the cooling regime.

Here I apply the formalism derived in §2 to clusters which contain a cooling flow. In this case, hydrostatic equilibrium no longer applies, and equation (9) must be

replaced with a set of cooling flow equations. I adopt the multiphase cooling flow equations discussed by Thomas (1998), who examines a quasihydrostatic, spherically symmetric flow with an emulsion of comoving but thermally isolated density phases. The Thomas (1998) scenario, summarized briefly in the Appendix, is a refinement of the classical multiphase models of Nulsen (1986).

The cooling flow equations have a free nondimensional parameter, k , which together with the gas emissivity ϵ completely specifies the shapes of the flow temperature, the mass deposition rate, and the gravitational potential. In the Thomas (1998) model, k describes, in an average sense, the nature of the phase mixture in the flow, and can have values from 1 to ∞ . Emulsions with $k = \infty$ include phases of arbitrarily low density; those with $k \sim 1$ allow only a small range of densities at each radius. Thomas (1998) argues that the $k \sim 1$ models are preferable because they reproduce observations of many cooling flow clusters where the emission-weighted temperature drops as $r \rightarrow 0$; on the other hand, the $k = \infty$ solutions have increasing $T(r)$ as $r \rightarrow 0$, in contrast with the observations.

Once k and the emissivity ϵ are specified, the resulting temperature and mass profiles constrain the anisotropy profile of the dark matter halo through equations (18)–(26). I will not use the β -model emissivity for the cooling flow calculations, first because it does not accurately match the observed emissivity profiles of cooling flow clusters, which are often cuspy as $r \rightarrow 0$, and also because it is inconsistent with all but the $k = \infty$ flows. Instead I use the broken power law

$$\epsilon(x) \propto (x^{\nu_1} + x^{\nu_2})^{-1}, \quad (49)$$

where $x \equiv r/r_c$ and $\nu_2 > \nu_1$. An emissivity profile with $\nu_1 = 0$ resembles a traditional β -model profile with $\beta = \nu_2/6$. See the Appendix for a detailed calculation.

Again, the first step in deriving the anisotropy profile is calculating β_{true} , the constant dark matter to gas energy ratio. Figure 9 shows the results. Here β_{true} depends strongly on the faint-end slope of the emissivity, ν_2 . When $\nu_2 \lesssim 3$, β_{true} is completely independent of ν_1 ; for $\nu_2 \gtrsim 3$, a slight perturbation exists as a function of ν_1 .

One interesting property of the solutions is that β_{true} never exceeds 0.65, because the multiphase equations do not allow larger values. The $k \sim 1$ models, which best match real clusters (Thomas 1998), allow the largest range of β_{true} ; the $k = \infty$ models always have $0.4 < \beta_{\text{true}} < 0.5$.

Figure 10 shows the resulting anisotropy profiles. A wide variety of profiles occur depending on the specific value of ν_1 , ν_2 , and k . However, all $\eta(r)$ begin positive and decline. When the emissivity is shallow— $\nu_2 = 2$, for example—the anisotropy tends towards negative values at larger radii. However, for reasonably steep emissivity profiles, the anisotropies stay constant or increase at large radii, and exhibit a substantial radial bias outside the core.

Although the cooling flow solutions extend to $r = \infty$, they have the greatest validity inside the cooling radius. If the measured emissivity of a cluster drops off very steeply at large radii ($\nu_2 \gtrsim 4$), no multiphase cooling flow solution can properly account for the gas physics at all radii. In such cases it is best to regard the true anisotropy parameter as resembling the cooling flow solution within the core, and the hydrostatic solutions (§3.3) for $r > r_c$.

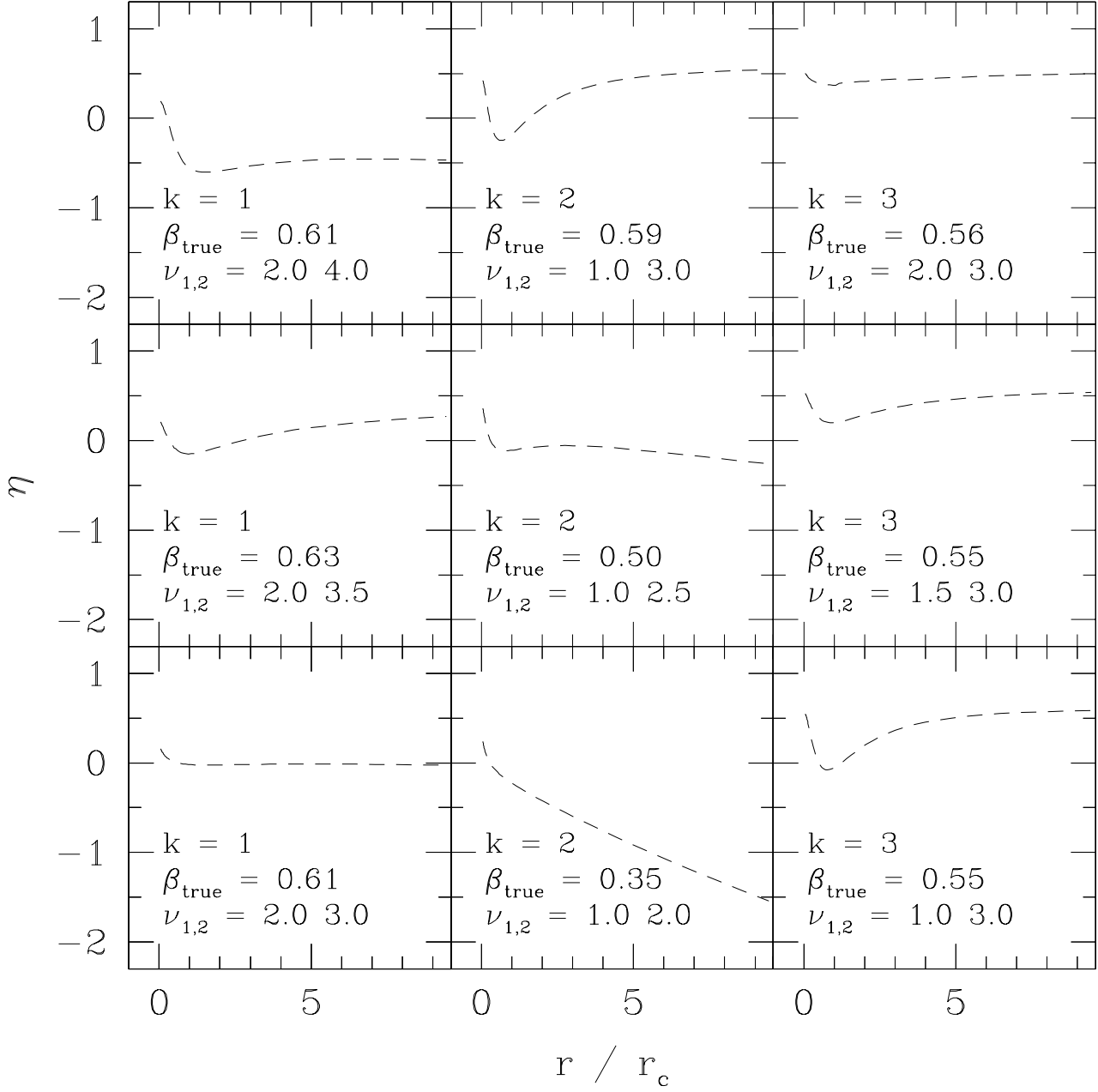


FIG. 10.— Anisotropy profiles for dark matter halos containing quasihydrostatic cooling flows with the indicated k -parameters. The emissivity profile characterized by ν_1 and ν_2 is given in equation (49). Also shown is $\beta_{\text{true}}(k, \nu_1, \nu_2)$.

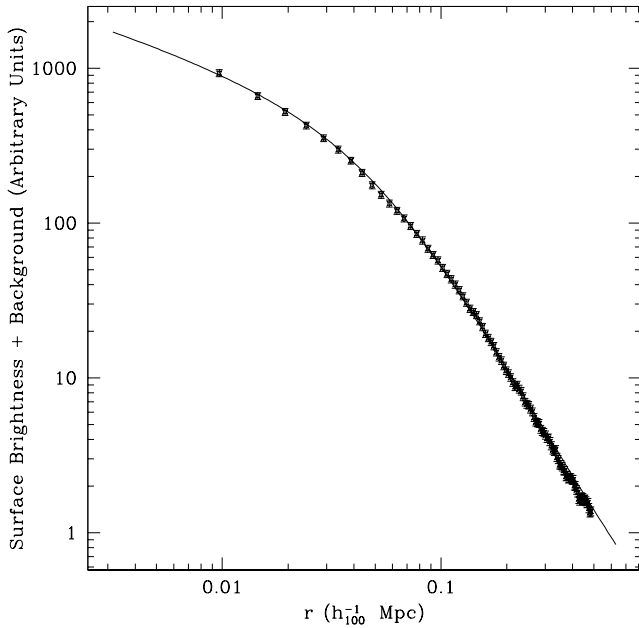


FIG. 11.— Surface brightness plus background for the *ROSAT* PSPC observation of Abell 2199. The error bars show the uncertainty due to photon noise plus a 5% additional error to account for uncertainty in the location of the bins. The solid line shown is the best fit combination of a constant background plus the projection of the broken power law from equation (49) along the line of sight, with $\nu_1 = 1.35$, $\nu_2 = 3.41$, and $r_c = 0.059h_{100}^{-1}$ Mpc.

4.2. Application to Abell 2199

Here I test the cooling flow anisotropy model by applying it to X-ray and optical observations of Abell 2199. I predict the shape and normalization of the projected velocity dispersion profile from the X-ray data, and compare it directly with independent optical spectroscopy. Here the cooling flow model determines the shapes of the mass and temperature profiles from the X-ray emissivity, and no additional lensing mass is required. An absolute temperature measurement provides the normalization.

Abell 2199 is a $z = 0.03$ cluster that contains a moderate cooling flow, with a mass deposition rate $\dot{M} \approx 150M_\odot \text{ yr}^{-1}$ (Peres et al. 1998). The *Einstein* observatory emission-weighted temperature is 4.5 ± 0.2 keV within $2h_{100}^{-1}$ Mpc (David et al. 1993). Velocity measurements for 98 galaxies in the field of the cluster are also available (Hill & Oegerle 1998).

To determine the shape of the X-ray emissivity, I examine a publicly available *ROSAT* PSPC observation of Abell 2199, with sequence identification RP800644N00, and a 41000 s exposure time. I use the MIDAS/EXSAS software package (Zimmermann et al. 1993) to calculate the surface brightness profile within $0.5h_{100}^{-1}$ Mpc. I then fit a constant background plus the surface brightness profile given by the projection of equation (49) along the line of sight. A deprojected emissivity with $\nu_1 = 1.35$, $\nu_2 = 3.41$, and $r_c = 0.06h_{100}^{-1}$ Mpc provides an excellent fit with a reduced chi squared equal to 0.6 (Figure 11). The errors on the fitted parameters are less than 10%. Note that the

innermost bin (not shown) is omitted from the analysis to minimize smearing of the emission due to the PSPC point spread function.

Once ν_1 and ν_2 are specified, the shapes of the temperature and mass profiles are fixed by the cooling flow equations. The David et al. (1993) temperature measurement fixes their normalization, and it is possible to fully calculate the velocity dispersion and anisotropy profiles. The line-of-sight velocity dispersion profile is then given by equation (48). To measure the profile independently from the Hill & Oegerle (1998) data, I apply the same procedure as that described in §3.4. The results of the analysis for both the $k = 1$ and $k = 2$ solutions are shown in Figure (12). For $k = 1$ $\beta_{\text{true}} = 0.62$, and for $k = 2$ $\beta_{\text{true}} = 0.57$. The profiles are steeper for larger values of k as $r \rightarrow \infty$.

Once again, this simple formalism provides an adequate description of the measured velocity dispersion profile without recourse to any free parameters. The reduced chi squared is 2.2, providing an acceptable fit for 9 degrees of freedom. Solutions with $k > 1$ are excluded by the data, because the velocity dispersion profile falls too quickly, affirming the intuition of Thomas (1998) that multiphase cooling flows with a broad density phase distribution are less likely to be consistent with real clusters.

5. CONCLUSION

I use the X-ray emission from hot gas embedded in a dark matter halo to break the degeneracy between the anisotropy parameter η and the system mass. Given an assumed mass profile and X-ray emissivity, the model simultaneously determines the anisotropy profile and the radial velocity dispersion profile. The resultant $\eta(r)$ for the hydrostatic case are consistent with anisotropy profiles from N-body simulations without gas. With the addition of central cooling flows, the formalism predicts a rich variety of anisotropy profiles within the cooling radius, most of which, however, contain a substantial radial anisotropy at the cluster center and at large radii.

I apply the formalism to two sets of observations of clusters of galaxies: the lensing cluster CL0024+16 and the cooling flow cluster Abell 2199. In both cases, the velocity dispersion profiles predicted by the anisotropy models are consistent with independently measured optical data. The agreement is particularly encouraging because no free parameters are allowed in the comparisons.

The warning of Binney & Tremaine (1987, p. 208), that for spherical systems, “radically different models can be consistent with both the Jeans equations and the observations,” is particularly applicable here and should not be neglected. This paper shows, however, that a combination of the X-ray emissivity and other auxiliary data, including the lensing mass or the gas temperature, provides a useful and self-consistent starting point for constraining the orbital structure of dark matter halos with gas.

This research was supported by the Smithsonian Institution. I thank Margaret Geller, Joseph Mohr, and the anonymous referee for suggestions that improved the paper considerably. I am grateful to Lars Hernquist, Kathleen Kang, and Daniel Koranyi for useful discussions.

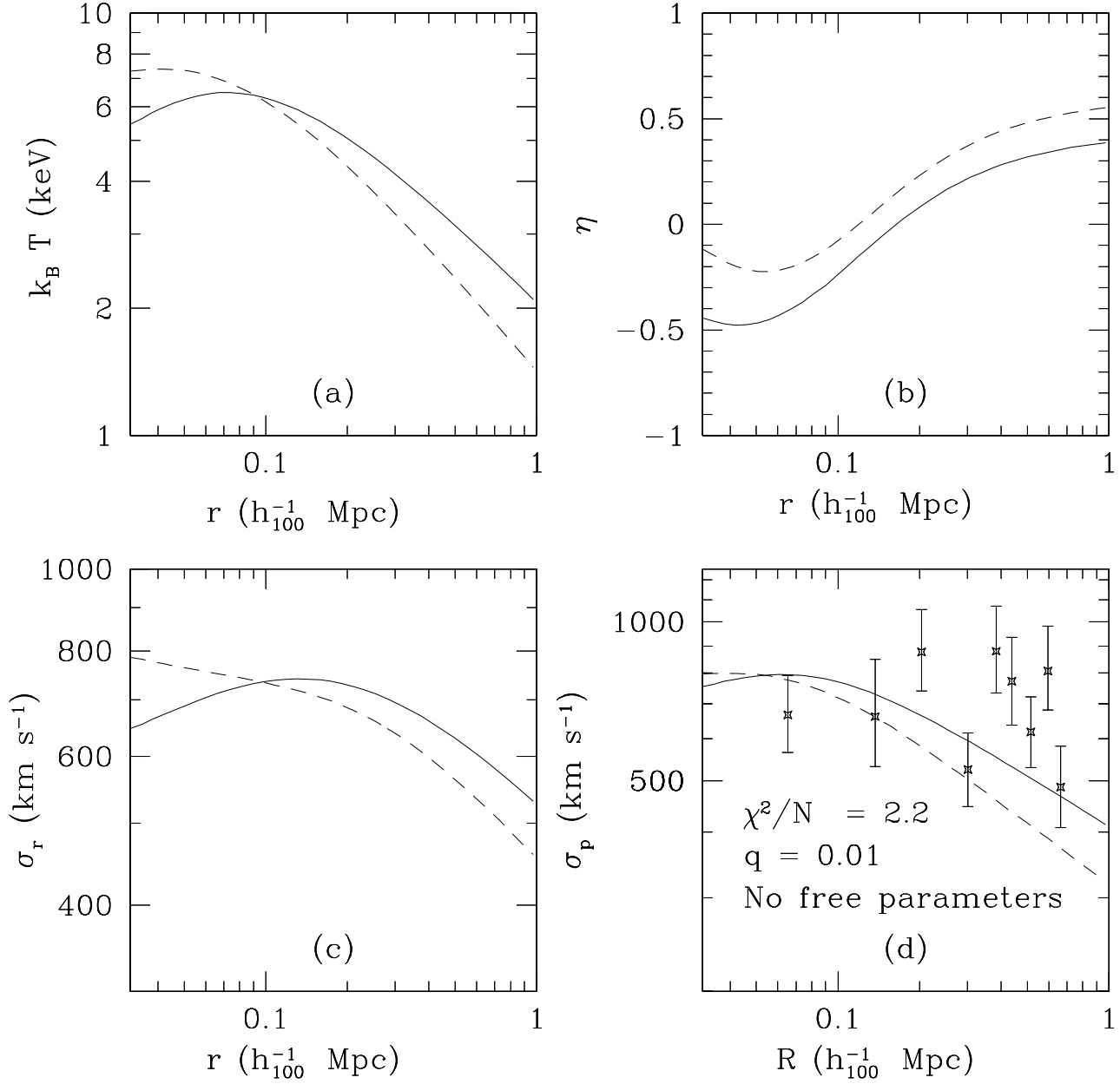


FIG. 12.— Derived properties of Abell 2199 for cooling flow solutions with $k = 1$ (solid lines) and $k = 2$ (dashed lines): (a) predicted plasma temperature; (b) predicted orbital anisotropy profile; (c) predicted three-dimensional radial velocity dispersion; (d) predicted line-of-sight velocity dispersion profile along with the measured galaxy velocity dispersion (Hill & Oegerle 1998).

REFERENCES

- Binney, J., and Tremaine, S. 1987, *Galactic Dynamics* (Princeton: Princeton University Press)
- Böhringer, H., Soucail, H., Mellier, Y., Ikebe, Y., & Schuecker, P. 2000, *A&A*, 353, L24
- Carlberg, R. G., Yee, H. K. C., Ellingson, E., Morris, S. L., Abraham, R., Gravel, P., Pritchet, C. J., Smecker-Hane, T., Hartwick, F. D. A., Hessler, J. E., Hutchings, J. B., & Oke, J. B. 1997, *ApJ*, 495, L13
- Cole, S., & Lacey, C. 1996, *MNRAS*, 281, 716
- David, L. P., Slyz, A., Jones, C., Forman, W., Vrtilik, S. D., & Arnaud, K. A. 1993, *ApJ*, 412, 479
- Diaferio, A. 1999, *MNRAS*, 309, 610
- Dressler, A., Smail, I., Poggianti, B. M., Butcher, H., Couch, W. J., Ellis, R. S., and Oemler, A., Jr. 1999, *ApJS*, 122, 51
- Eke, V., Navarro, J. F., & Frenk, C. S. 1998, *ApJ*, 503, 569
- Geller, M. J., Diaferio, A., & Kurtz, M. J. 1999, *ApJ*, 517L, 23
- Gerhard, O., Jeske, G., Saglia, R. P., & Bender, R. 1998, *MNRAS*, 295, 197
- Hernquist, L. 1990, *ApJ*, 356, 359
- Hill, J. M. & Oegerle, W. R. 1998, *AJ*, 116, 1529
- Jones, C., & Forman, W. 1984, *ApJ*, 276, 38
- Kauffmann, G., Colberg, J. M., Diaferio, A., White, S. D. M. 1999, *MNRAS*, 303, 188
- Mahdavi, A., Geller, M. J., Böhringer, H., & Ramella, M. 1999, *ApJ*, 518, 69
- Markevitch, M., Forman, W. R., Sarazin, C. L., & Vikhlinin, A. 1998, *ApJ*, 503, 77
- Merritt, D. 1985, *AJ*, 90, 1027
- Metzler, C. A., White, M., Michael, N., & Loken, C. 1999, *ApJ*, 520, L9
- Mohr, J. J., Mathiesen, B., & Evrard, A. E. 1999, *ApJ*, 517, 627
- Navarro, J. F., Frenk, C. S., & White, S. D. M. 1997, *ApJ*, 490, 493
- Nulsen, P. E. J. 1986, *MNRAS*, 221, 377
- Peres, C. B., Fabian, A. C., Edge, A. C., Allen, S. W., Johnstone, R. M., & White, D. A. 1998, *MNRAS*, 298, 416
- Sarazin, C. L. 1988, *X-ray Emission from Clusters of Galaxies* (Cambridge: Cambridge University Press)
- Soucail, G., Ota, N., Böhringer, H., Czoske, O., Hattori, M., & Mellier, Y. 2000, *A&A* in press (astro-ph/9911062)
- Thomas, P. A. 1998, *MNRAS*, 299, 349
- Tyson, J. A., Kochanski, G. P., & Dell’Antonio, I. P. 1998, *ApJ*, 498, L107
- van der Marel, R. P., Magorrian, J., Carlberg, R. G., Yee, H. K. C., & Ellingson, E. 2000, *AJ*, 119, 2038
- Xue Y. & Wu, X. 2000, *ApJ*, in press
- Zimmermann, H. U., Belloni, T., Izzo, C., Kahabka, P., & Schwentker, O. 1993, in *ASP Conf. Ser. 52: Astronomical Data Analysis Software and Systems II*, p. 53

APPENDIX

DERIVATION OF THE ANISOTROPY PROFILE FROM THE COOLING FLOW EQUATIONS

Thomas (1998) derives equations that describe a quasihydrostatic, spherically symmetric flow consisting of an emulsion of comoving but thermally isolated density phases. The relevant variables are the mass, M , the temperature, T , the emissivity, ϵ , the mass accretion rate, \dot{M} , and the following dimensionless quantities:

$$\Sigma \equiv \frac{GM\mu m_p}{2rk_B T}, \quad (\text{A1})$$

$$\tau \equiv \frac{1}{k} \frac{d \ln \dot{M}}{d \ln r}, \quad (\text{A2})$$

$$\chi \equiv \frac{d \ln M}{d \ln r}, \quad (\text{A3})$$

where k_B is Boltzmann's constant, and k is a dimensionless parameter that characterizes the range of densities present at each radius. The $k = 1$ models possess a minimum density at each radius and are the least extended. The $k = \infty$ models include phases of arbitrary low density, and are the most extended convectively stable distributions.

With the assumption that the cooling function is dominated by thermal bremsstrahlung ($\Lambda \propto \rho_g^2 T^{1/2}$) and that the ratio of specific heats $\gamma = 5/3$, the Thomas (1998) steady-state equations have the solutions

$$\tau = \frac{r^3 \epsilon^{5/7}}{(20/21 + k) \int r^2 \epsilon^{5/7} dr}, \quad (\text{A4})$$

$$\Sigma = -\frac{5}{14} \left(\tau + \frac{d \ln \epsilon}{d \ln r} \right), \quad (\text{A5})$$

$$\chi = 1 - \frac{4}{5} \Sigma + \frac{2}{3} \tau + \frac{d \ln \Sigma}{d \ln r}. \quad (\text{A6})$$

Rearranging the equations to solve for the temperature yields

$$T \propto \epsilon^{2/7} \left[\left(\frac{20}{21} + k \right) \int r^2 \epsilon^{5/7} dr \right]^{\frac{20}{20+21k}}, \quad (\text{A7})$$

where the expression in square brackets approaches 1 as $k \rightarrow \infty$. It is therefore evident that for all reasonable emissivity profiles, the $k = \infty$ solutions have $dT/dr < 0$ everywhere.

Once the temperature is fixed, it is possible to constrain β_{true} , the ratio of the total dark matter kinetic energy to the gas energy. Because $4\pi r^3 \rho_{\text{dm}} = M\chi$, the velocity dispersion equations (19)–(20) become

$$\sigma_1^2 = \frac{k_B}{m_p \mu r T \Sigma \chi} \int 3\beta_{\text{true}} T^2 \Sigma \chi dr, \quad (\text{A8})$$

$$\sigma_2^2 = \frac{k_B}{m_p \mu r T \Sigma \chi} \int 2T^2 \Sigma^2 \chi dr. \quad (\text{A9})$$

In cases where $\sigma_1^2 \gg k_B T / (m_p \mu)$ at large radii, β_{true} once again takes on a unique value:

$$\beta_{\text{true}} = \lim_{r \rightarrow \infty} \frac{\sigma_2^2}{3\sigma_1^2}. \quad (\text{A10})$$

If the integrals in equations (A8)–(A9) diverge as $r \rightarrow \infty$, then, applying l'Hôpital's rule,

$$\beta_{\text{true}} = \frac{2}{3} \lim_{r \rightarrow \infty} \Sigma. \quad (\text{A11})$$

$$= -\frac{5}{21} \left[\frac{3}{20/21 + k} + \lim_{r \rightarrow \infty} \frac{d \ln \epsilon}{d \ln r} \left(\frac{5}{20/3 + 7k} + 1 \right) \right]. \quad (\text{A12})$$

If, on the other hand, the integrals converge, then β_{true} must be determined numerically. After this, direct application of equations (18) and (26) will yield the radial velocity dispersion profile σ_r and the anisotropy profile $\eta(r)$.